JOURNAL OF MATERIALS SCIENCE 30 (1995) 6119–6135

Liquid phase bonding of siliconized silicon carbide

A. C. FERRO*, B. DERBY
Department of Materials, University of Oxford, Parks Road, Oxford OX1 3PH, UK

Aluminium was used as a braze to join siliconized silicon carbide to itself. Brazes were carried out in the 700–1100 °C temperature range, in vacuum. A thick reaction layer forms in the ceramic adjacent to the braze film, due to reaction between the metal braze and the free silicon present in the ceramic matrix. The silicon concentration of the braze film reaches values well above the maximum liquid solubility at the brazing temperature. A pseudo-transient aluminium–silicon liquid phase promotes the formation of a 100% silicon braze film when either high temperatures, long holding times or very slow cooling rates are used. The dominant mechanism responsible for the formation of the braze microstructure is the preferential unrestrained solidification growth of Si plates on the braze plane, supported by fast liquid Si diffusion. Strong joints were produced and, when pure silicon brazes formed, four-point bend strengths over 200 MPa were obtained at testing temperatures as high as 700 °C. Fracture occurs either in the reaction layer–ceramic boundary or in the braze, the crack propagation plane changing from one side of the braze–ceramic interface to the other and through the braze itself.

1. Introduction

The potential use of ceramics as structural materials strongly depends on the establishment of reliable processes permitting ceramics to be joined to themselves and to metals. The formation of successful metal–ceramic joints depends on the achievement of intimate contact between the two materials and the conversion of this contact into an atomically bonded interface. Ceramics have low toughness and very limited plastic capability. They generally have much higher elastic moduli and lower coefficients of thermal expansion than metals. Successful joints thus depend on the ability of the system to accommodate the thermal expansion mismatch stresses generated during cooling after fabrication or as a result of temperature changes in service [1, 2].

Silicon carbide is a very promising material for use in structural applications from consideration of stability and strength at elevated temperature. It also has a very low coefficient of friction and wear resistance in contact with itself and with many other surfaces. Siliconized or reaction bonded silicon carbide, RBSiC, initially developed as a nuclear fuel cladding material, is now a major engineering ceramic. It is fabricated through a low cost process, low temperatures (1400–1500 °C) are used during manufacture (sintered SiC, SSiC, requires temperatures in the 1900–2100 °C range), no pressure or additives are needed, almost no shrinkage occurs during fabrication, and a fully dense ceramic is made. Its good thermal conductivity and low coefficient of thermal expansion provides high thermal shock resistance, a fundamental requirement for many elevated temperature applications. Its friction and wear properties also make it an attractive material for bearing and sealing applications at room or high temperatures. It is used for a variety of mechanical seals, bearings and spinnerets [3].

Since the early 1980s attempts have been made to produce strong SiC–SiC joints. The best results were obtained using brazing and diffusion bonding techniques.

In diffusion techniques two bodies of silicon carbide are placed together after grinding and polishing flat and parallel, with or without interlayers, and heated to a temperature just below the melting or solidus temperature of the interlayer used and of the materials to be joined. The assembly is subjected to a high pressure (1–10 MPa) and is generally held in vacuum. Several interlayers have been tried in order to bond SiC to itself sometimes producing high bend strengths (maximum value 490 MPa [4]).

Brazing techniques use assemblies of thin metal foils placed between the bodies to be joined. Temperatures above the melting or liquidus temperatures of the metal or alloy are used. No, or only a very light pressure is applied. The assembly is generally held in a high vacuum during the whole thermal cycle. Brazing is a very attractive joining technique because low temperatures, no pressure and only little surface preparation is required to obtain a joint. In addition it

* *Present address*: Departamento de Engenharia de Materiais, Instituto Superior Técnico, Avenida Rovisco Pais, 1, 1096 Lisboa Codex, Portugal.

presents very few problems in scaling up from the laboratory to industrial batch production. Vacuum brazing is commonly used to join metal components and its use in metal–ceramic applications should present few problems for the process. Wettability is a dominant factor when brazing is considered. It is well established that for preplaced metallic foil brazes a contact angle of $\theta < 70°$ is necessary for most joining applications [5].

Current active braze alloys use titanium additions to silver–copper eutectic alloys or to pure silver. These alloys tend to react strongly with many ceramics, particularly SiC, forming brittle interfacial phases. They have low ductility and poor oxidation and corrosion resistance [6]. They have been used to join SiC to itself in the temperature range 800–1000 °C [7–9]. High bond strengths have been obtained, but complex reaction layers containing TiC, Ti_5Si_3 or Ti_3Si_2 form at the interface.

Aluminium and aluminium base alloys brazes with small additions of silicon, titanium and copper have been proposed given the tendency of Al to react with oxygen, nitrogen and carbon. Strong bonds and good wettability with many ceramics, particularly silicon base ceramics, have been reported [10]. These aluminium braze alloys are more ductile, and more corrosion and oxidation resistant than the established active metal brazes. However, they have lower temperature capability. Their application is considered limited to temperatures, $T < 300$ °C. Also, particular importance has to be given to the reaction between SiC and Al–Si alloys and to the conditions for Al_4C_3 formation. This reaction is of great importance from the technological point of view because of the poor corrosion resistance and brittleness of Al_4C_3. Fig. 1 shows an isothermal section of the Al–Si–C ternary phase diagram, an Al–Si melt is in equilibrium with SiC only above some critical Si concentration. The variation with temperature of this critical silicon concentration needed to avoid Al_4C_3 formation has been determined by several workers both theoretically and experimentally [11–16] (Fig. 2).

Aluminium alloys wet many non-oxide ceramics. Aluminium and aluminium–silicon alloys are known to wet SiC very well under vacuum conditions [17, 18]. Also, depending on the alloy composition, they can exhibit extensive ductility. They can be used at lower temperatures than copper–silver alloys and interface reactions are more easily controlled. Their prospective use as braze interlayers for metal–ceramic joining seems promising. Japanese researchers have used aluminium and aluminium foils clad with Al10Si as a braze for SSiC and RBSiC [14, 19–21]. Vacuum and temperatures in the 600–1000 °C range were used. High bond bend strengths were obtained: 240 MPa for SSiC and 110 MPa for RBSiC. Most results so far published on joining SiC materials use either pressureless sintered or hot pressed material [2, 22–29]. Only a few results have been reported on the joining of siliconized SiC. The methods used and results obtained in these previous studies are summarized in Table I.

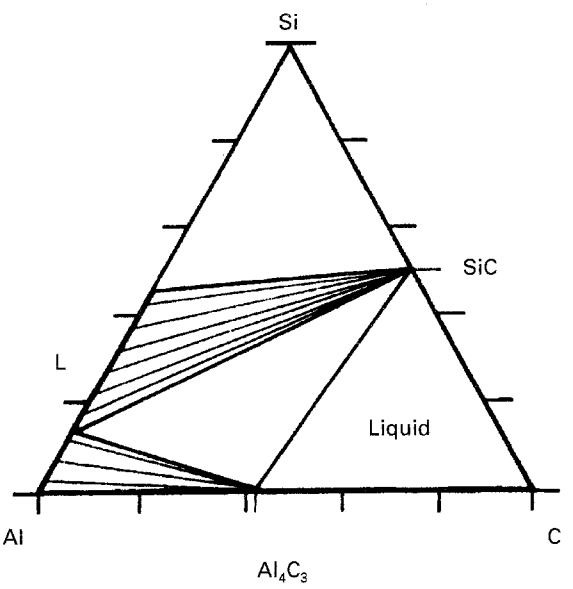

Figure 1 Isothermal section of metastable Al–Si–C phase diagram at 1000 °C.

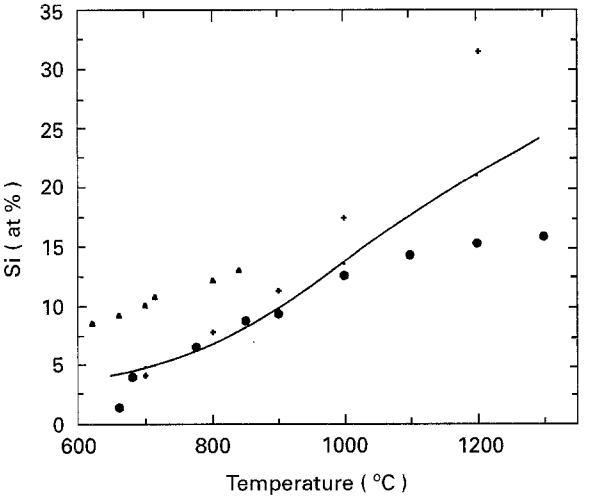

Figure 2 Variation with temperature of the silicon concentration of the liquid phase in equilibrium with Al_4C_3 and SiC. Experimental and theoretical values. (—) Nakae [16], (+) Iseki [14], (▲) Lloyd [15], (●) Viala [12].

In this paper the use of a pure aluminium braze for joining reaction bonded silicon carbide has been investigated. From the binary Al–Si phase diagram [33] (Fig. 3) one would expect the high Si content present between the SiC grains to dissolve into the molten Al braze up to a concentration defined by the temperature used. This relatively high Si content should prevent the formation of any unwanted Al_4C_3 and also result in widely dispersed Al islands in any reaction zone. Experiments were carried out to identify suitable thermal cycles and brazing conditions. Joint quality was assessed by mechanical testing from room temperature and up to 700 °C. Optical microscopy, scanning electron microscopy (SEM) and electron probe microanalysis (EPMA) were used to characterize the braze microstructure. Fracture surfaces were also examined using SEM.

TABLE I Data on reaction bonded silicon carbide joining

Material	Interlayer	Joining method atmosphere (Pa)	Joining parameters			Mechanical properties (MPa)			Interface reaction layers Thickness (in parenthesis μm)	Reference
			Temperature (°C)	Time (min)	Pressure (MPa)	Four-point bending	Shear	Testing, T (°C)		
RBSiC (12% Si)	Ge powder final braze thickness 20 μm	Vacuum brazing	1180	10		160 ± 40 190 ± 30 245 ± 25 235 ± 60		r.t. 500 700 900	Ge rich braze layer + thick reaction zone with a SiGe solid solution (300–500)	[30]
RBSiC (12% Si)	Ge powder final braze thickness 200 μm	Vacuum brazing	1180	10		65 ± 5 110 ± 5 120 ± 10 165 ± 10 50 ± 10		r.t. 500 700 900 1000	Ge rich braze layer + thick reaction zone with a SiGe solid solution (300–500)	[30]
RBSiC (10% Si)	Al metal foil (500 μm)	Vacuum brazing (10^{-2})	800	2–3		110 ± 25 145 ± 50 100 ± 5 20 ± 5		r.t. 200 400 550	Some Si rich zones in the braze layer + thick Al–Si rich ceramic reaction zone (200)	[20]
			1000	2–3		120 ± 25 80 ± 20 85 ± 20 65 ± 5		r.t. 200 400 550	Many Si rich zones in the braze layer + thick Al–Si rich ceramic reaction zone (500)	
RBSiC (13% Si)	Nb metal foil	Diffusion bonding vacuum (13×10^{-3})	1400	120	2.0 1.0 0.5		90 72 37	r.t. r.t. r.t.	Nb_5Si_3	[31]
			1400	120	1.5		77 65 57 54	r.t. 200 500 800		[32]

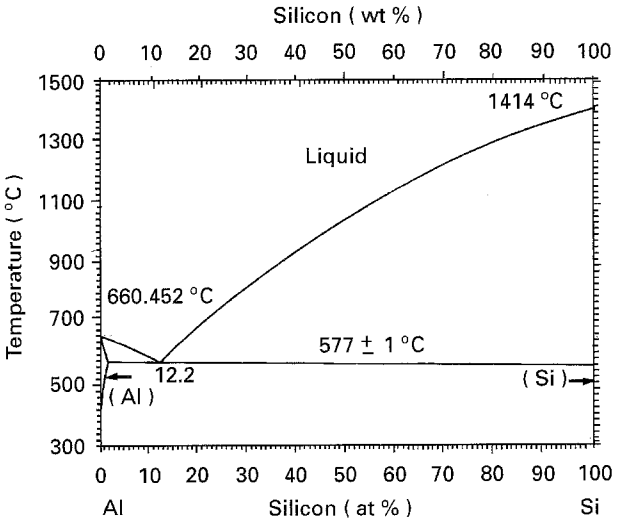

Figure 3 Binary Al–Si phase diagram [33].

2. Experimental procedure

2.1. Starting materials

RBSiC was supplied in the form of approximately 15 mm diameter bars (TenMat, UK). Stubs, 14 mm long, were cut from these bars. These were lapped on metal plates using diamond slurries of a range of sizes down to 3 μm to ensure flatness. Prior to brazing, discs were lapped again with 3 μm diamond paste, to minimize the effects of surface oxidation, and finally ultrasonically cleaned with acetone.

The microstructure was assessed using SEM and optical microscopy. The secondary electron contrast obtained in the SEM (Fig. 4a) allows a good distinction between the α-SiC seeds, ≈5–10 μm (dark grey with angular shapes), the α epitaxial layer surrounding them (white or light grey, with a sharp interface with the α-seeds and an irregular contour in the outside interface), and the β-type, intergranular SiC grains. The silicon matrix network appears black. Optical micrographs (Fig. 4b) reveal a two phase structure of silicon (light) and silicon carbide (darker) and were used to determine the volume fraction of the silicon phase as 18.6 ± 1.2%. This RBSiC material shows very limited porosity. A large scale feature formed by areas of high SiC volume fraction, regularly distributed throughout the bars, with a characteristic dimension of 200 μm was found. The room temperature four-point bend strength of the bulk RBSiC material was determined to be 411 ± 38 MPa (from an average of 24 specimens).

A 0.5 mm thick pure Al sheet (Goodfellow Metals), with an impurity content less than 10 p.p.m., was further cold rolled to 0.4 mm. Discs of 15.5 mm diameter were cut from the sheets and trimmed. Before brazing, these were abraded with a 600 grit silicon carbide paper, to produce a final thickness around 0.3 mm, pickled in a 10% NaOH–water solution for 10 min, rinsed in distilled water and ultrasonically cleaned in acetone.

2.2. Equipment and methods

2.2.1. Brazing

All brazing experiments were carried out in a vertical vacuum furnace heated by a molybdenum element. A turbomolecular pump system ensured vacuum levels better than 10^{-3} Pa during high temperature brazing, generally 2×10^{-4} Pa was obtained. A molybdenum jig was designed to ensure alignment between the pieces to be joined and to avoid contamination from the fixing devices. This also assisted the brazing with a small pressure (≈2.5 kPa from its own weight) that was found to be beneficial. No Mo contamination was ever found in the braze film.

A standard thermal cycle was used for every brazing experiment, with variations in the terminal brazing temperature, holding time and cooling rates. A heating rate of 40 °C min^{-1} and a 30 min preheating stage at a temperature $T_1 = 500$ °C were selected. Brazing temperatures were between 700 and 1100 °C, holding times were of 0, 30, 90 and 240 min, and four different cooling rates, 0.4 and 4 °C min^{-1}, the natural cooling rate of the furnace (NCR) and helium quenching were used. These last two methods provide cooling rates of around 20–40 and 400 °C min^{-1}, respectively, when cooling from 1000 °C. The gas quenching apparatus has a cylindrical chamber into which the braze assembly is lifted for quenching, and a high vacuum gate

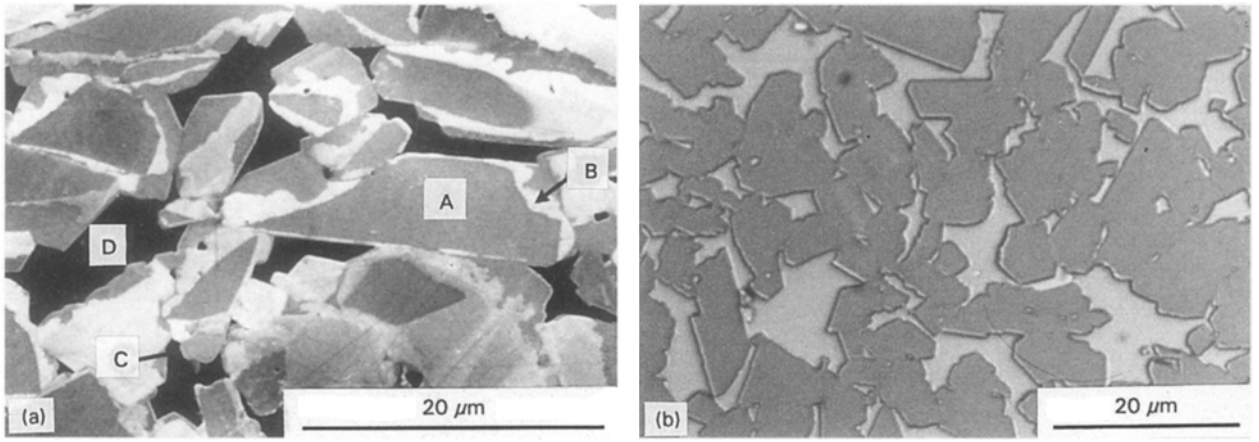

Figure 4 Microstructure of reaction bonded "Refel" SiC from TenMat, RBSiC: (a) SEM, secondary electron contrast, showing α-seeds, marked A, the whiter epitaxial layer, arrow B, intergranular SiC, arrow C and the black silicon matrix, marked D; and (b) optical, enhancing the contrast between the silicon network matrix, light grey, and the SiC grain structure, darker grey.

valve that isolates the quenching area from the main furnace. This allows faster and efficient cooling. Helium is forced through the system at 35 kPa pressure.

2.2.2. Mechanical testing

The brazed joints were sliced into bars of approximately $3 \times 3 \times 28$ mm for four-point bend tests. To ensure reproducible results a uniform preparation procedure was used. Square bars were lapped with a 3 μm diamond slurry. Deviations from parallelism of less than 0.1° were achieved. Tension edges were flattened using 8 μm diamond slurry by light lapping with small brass holders. All specimens were inspected with a stereomicroscope to identify any damage before testing.

Room temperature tests were carried out in four-point bend at a crosshead speed of 100 μm min^{-1} and upper and lower spans of 24 and 6 mm, respectively, were selected. Higher temperature tests were carried out using a crosshead speed of 10 μm min^{-1} and upper and lower spans of 16 and 8 mm respectively were selected. All tests were performed in air and specimens were held for 1 h at the test temperature before straining. Specimens were tested at 300, 500 and 700 °C.

2.2.3. Fractography

The fracture surfaces were first macroscopically characterized according to failure nature and path of crack propagation. Six different types were identified: A, B and C corresponded to rapid catastrophic brittle failure. In B (braze) failure occurred in the braze region, parallel to the braze plane; in C (ceramic) crack propagation took place in the ceramic, far away from the metal–ceramic interface; A corresponded to a mixed path: the crack was generally initiated in the ceramic, as in C, but deflected when it reached the braze region to propagate parallel to the braze plane, as in B. D type fracture had a catastrophic–ductile transition, leading to crack propagation arrest. After the maximum load the specimen resistance dropped to variable finite values, and crack propagation occurred with a small decrease in applied load. Failure occurred in the braze region parallel to the braze plane, as in B. In cases E and F crack propagation was initiated near the boundary between a thick reaction zone and the ceramic. It then either (type E fracture) propagated parallel to that interface, possibly changing plane, or (type F fracture) formed a typical cup-shape surface. This shorthand form of A–F will be used throughout to identify the type of fracture.

3. Results

3.1. Braze microstructure

There have been a few previous studies on the interaction between pure Al and RBSiC [20, 34, 35]. Some of these reports [34, 35] did not reproduce the brazing environment; instead are small pieces of RBSiC immersed in liquid Al. Al partially replaces the Si phase in the ceramic and a low Si content Al–Si liquid is obtained. At high temperatures (around 1000 °C) Al_4C_3 forms in abundance at the SiC–liquid interface [35]. Iseki *et al.* studied this interaction using a configuration of an Al sheet between two ceramic pieces [20] and observed a different behaviour. A thick reaction zone developed in the ceramic where an Al–Si liquid replaced the interconnecting Si phase, and a Si rich Al–Si liquid crystallizes in the braze layer. Reaction layers 200 and 500 μm thick formed at 800 and 1000 °C, respectively, with a RBSiC ceramic containing 13.3 vol % free Si. The amount of Si found in the braze layer also increased significantly with temperature without Al_4C_3 formation.

In the present experiments, the amount of Si found in the braze layer also increases sharply with brazing temperature. Al diffuses into the ceramic through the dissolution of the free Si producing a well defined thick reaction zone. This contains the primary SiC grains, which remain basically untouched, and an Al rich Al–Si two phase region replaces the free Si network of the RBSiC material. Fig. 5 presents a typical Al–K_α EPMA map of a joint that illustrates the described microstructure. The thickness of the reaction layer and the composition of the Si rich braze layer were studied as functions of brazing time and temperature. Si concentrations were measured using quantitative metallography. The volume fractions of eutectic and primary Si existing in the braze film were determined and converted into weight percentages. The reaction zone thickness was directly measured by optical microscopy. The values stated here are the average results of measurements made on one to four specimens extended to all cross-sections obtained for each specimen.

3.1.1. The effect of brazing temperature and time

The variation, with time and temperature, of the silicon concentration in the braze layer and of the reaction zone thickness is presented in Figs 6 and 7, respectively. From Fig. 6a, it is apparent that in every case the Si content is well in excess of the equilibrium value. This deviation increases with temperature and, at 1000 °C, an almost pure Si layer is repeatedly observed. At 1000 °C, for the conditions used here, time seems to have no effect and only a small increase of Si concentration with time can be found for the experiments at 880 °C (Fig. 6b). The reaction zone thickness results (Fig. 7a) are much more scattered, particularly at lower temperatures. Nevertheless, a net increase, from ≈400 to ≈1100 μm, can be seen as the brazing temperature increases from 880 to 1100 °C. Brazing time seems to have little effect on the values obtained.

A theoretical reaction zone thickness, Z_t, can be calculated if it is assumed that a homogeneous liquid, with an Si concentration, C_{Si}, corresponding to a binary saturated Al–Si liquid for a given temperature completely replaces the interconnected Si phase of the RBSiC ceramic. These, calculated from an Al mass balance, depend only on the mass of Al involved in the process, here expressed as a "real" braze thickness, Z_B, and on temperature. These can be expressed as an

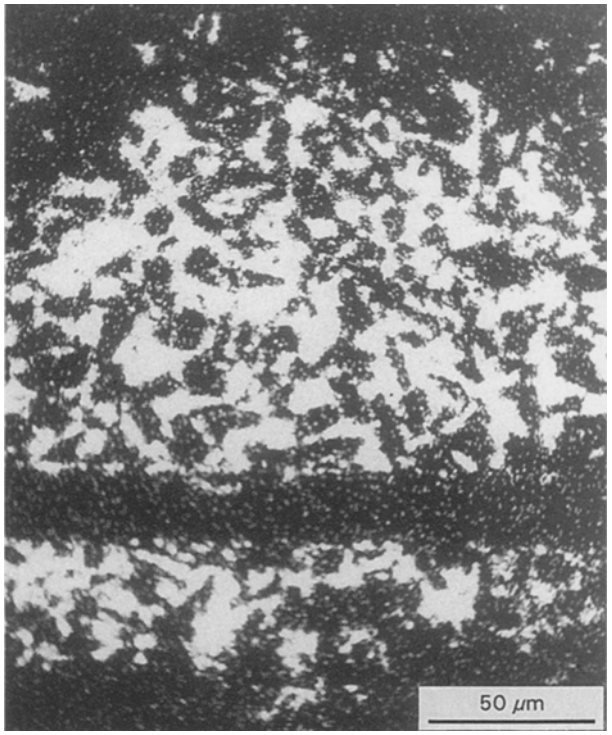

Figure 5 RBSiC vacuum brazed with Al at 880 °C for 90 min. Al–K_α EPMA picture showing an Al rich reaction zone and an almost pure Si braze.

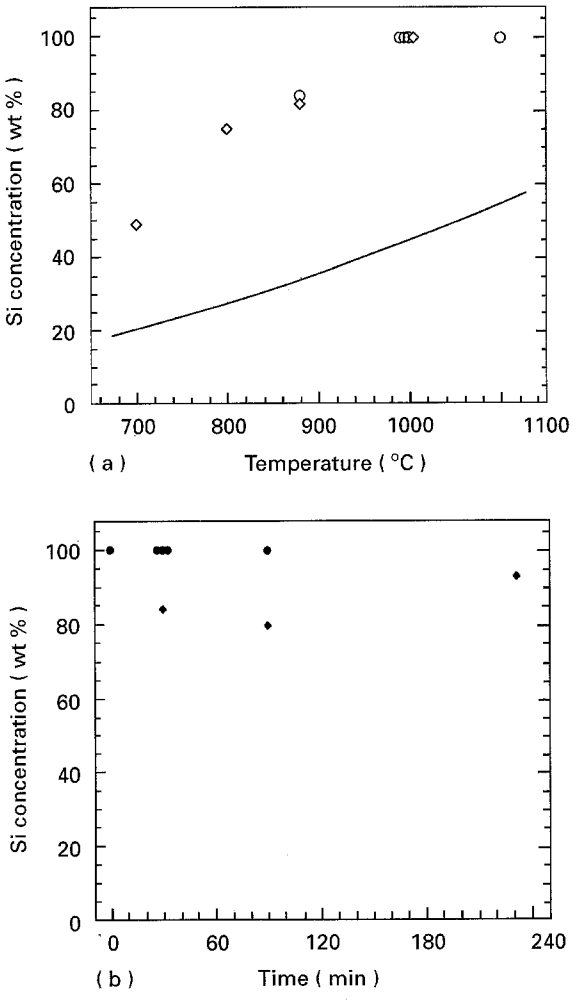

Figure 6 RBSiC vacuum brazed with Al. Variation of the Si concentration in the braze layer with (a) temperature and (b) time. The solid line represents the equilibrium Si concentrations predicted by the Al–Si binary phase diagram. (○) 30 min, (◇) 90 min, (●) 1000 °C, (◆) 880 °C.

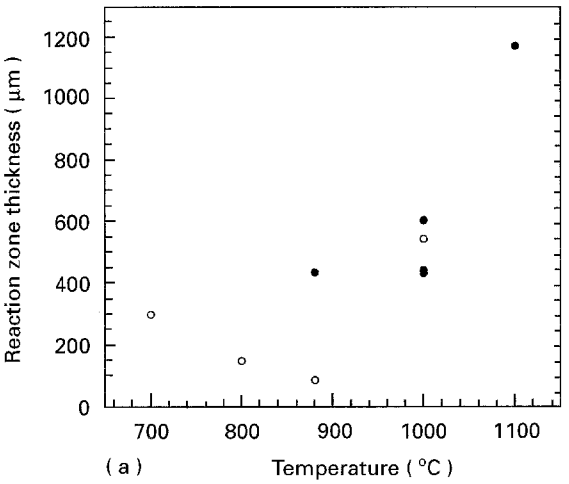

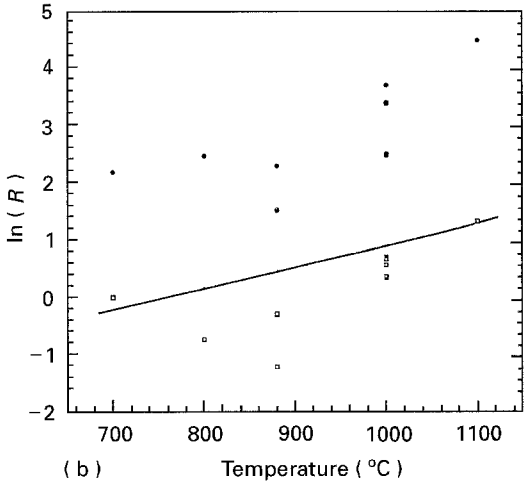

Figure 7 RBSiC vacuum brazed with Al. Variation of the reaction zone thickness with temperature and time: (a) absolute values, (b) thickness ratios: (□) R_i and (●) R_f correspond to minimum and maximum experimental values. The solid line represents the ideal ratio, R^*. (●) 30 min, (○) 90 min.

ideal, dimensionless, reaction zone thickness ratios, $R^* = Z_t/Z_B$ given by Equation 1

$$R^* = \frac{Z_t}{Z_B} = 3.115\frac{C_{Si}}{1 - C_{Si}} \quad (1)$$

The calculated R^* values and the corresponding Z_t thickness for arbitrarily chosen Z_B values are presented in Table II.

Minimum and maximum experimental thickness ratios can be proposed if it is assumed, that either all the Al present in the initial 300 μm thick braze discs, or only that corresponding to the thickness of the final braze layer after joining, are responsible for the formation of the reaction zone. The variation with temperature of R_i, minimum value corresponding to the initial braze thickness, and R_f, maximum value corresponding to the final braze thickness, are plotted in Fig. 7b with the ideal calculated ratios, R^*. These results show considerable experimental scatter either side of the calculated value. However, the mean reaction layer thickness is always wider than expected and the deviation appears to increase with temperature above 880 °C. The scatter can be partly explained by

TABLE II Variation with temperature of the ideal reaction zone thickness ratio, R^*, and corresponding theoretical thickness, Z_t, for different values of Al braze thickness, Z_B.

Temperature (°C)	R^*	Z_B (μm)			
		20	50	100	300
700	0.813	16	41	81	244
800	1.211	24	61	121	363
900	1.760	35	88	176	528
1000	2.549	51	128	255	768
1100	3.807	76	190	380	1142
1200	6.074	121	304	607	1822

the observation that extruded droplets sometimes form to one side of the assembly which result in a lower Al content than expected. This would, however, result in a smaller reaction zone side and not the positive deviation seen in Fig. 7b.

Typical low magnification micrographs of the structures obtained for this set of experiments are presented in Fig. 8. Si solidifies as coarse slabs that occupy the whole braze thickness. The Al–Si eutectic is pushed between these into regions that also occupy the whole braze thickness. The SiC–Si braze interface is remarkably undisturbed by the joining process. In the reaction zone, areas of high and low concentration of Al–Si eutectic can be observed. The thinner networks between the SiC interconnected structure tend to be preferentially filled with the eutectic structure (Fig. 9).

Another feature of interest in the braze is the grain size of the Si slabs formed in the braze film under NCR conditions. The Si grain size can be assessed by studying cleavage markings on the joint fracture surfaces. When the fracture propagates through the braze plane it generally runs inside the braze, cutting the Si slabs, and producing clear {1 1 1} cleavage surfaces. From these, Si slabs at least as long as 500 μm, at 800 °C, and longer than 1 mm, at 1000 °C, can be identified (Fig. 10).

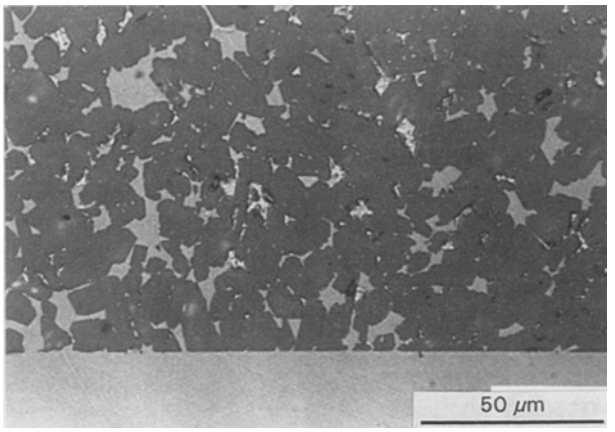

Figure 9 Detail of the RBSiC–Al reaction zone showing areas of low and high Al–Si eutectic density (1000 °C, 30 min). Note the preferential occupation of thinner regions of the interconnected matrix network by the eutectic.

3.1.2. The effect of cooling rate

The variation of the silicon concentration in the braze layer with cooling rate is presented in Fig. 11. The results obtained for the joints brazed at 880 °C for 30 min show that the cooling rate has a clear effect, and 100% silicon layers can be obtained at very low cooling rates. For the quenched sample a value of ≈75% Si was obtained, which is clearly above the saturation value of a binary Al–Si liquid at that temperature. At 1000 °C the variation is not so apparent and, with a 30 min holding time, only a small decrease, from 100% Si to ≈92% Si, is observed. However, a major decrease in Si content is observed for the zero holding time samples, from 100% for the natural cooling rate to 65% for the quenched sample. The variation with cooling rate of the reaction zone thickness and thickness ratios is presented, respectively, in Fig. 12. At either 880 or 1000 °C when the 30 min time interval is used, a real increase in these parameters is observed for the quenched samples and no variation can be established between the other cooling rates.

The results obtained for the 1000 °C experiments are illustrated by the micrographs presented in

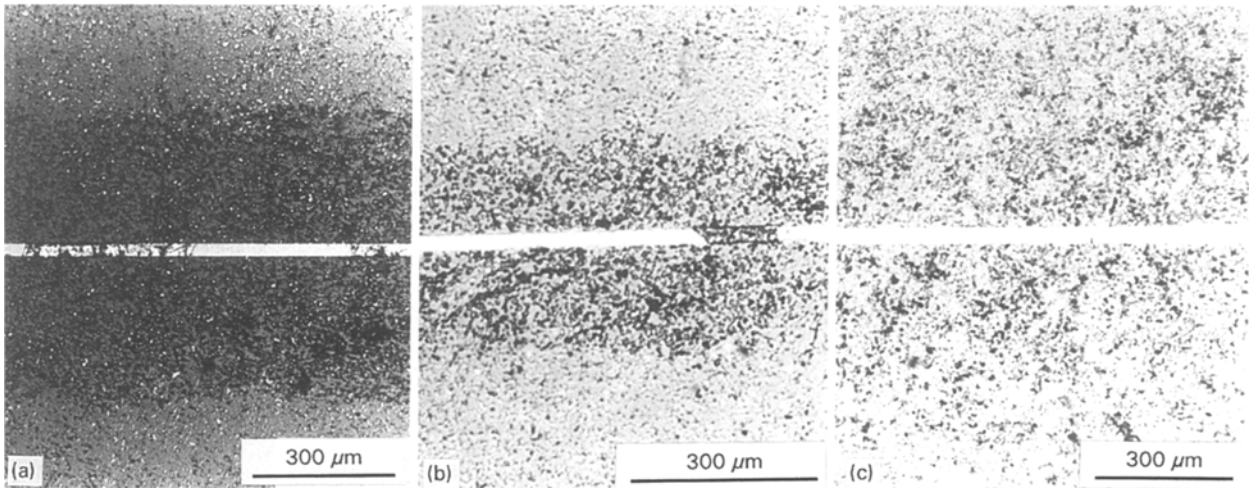

Figure 8 RBSiC–Al joint microstructures vacuum brazed and naturally cooled inside the furnace: (a) 700 °C, (b) 880 °C, and (c) 1000 °C. Note the formation and evolution of the Al–Si areas in the braze film.

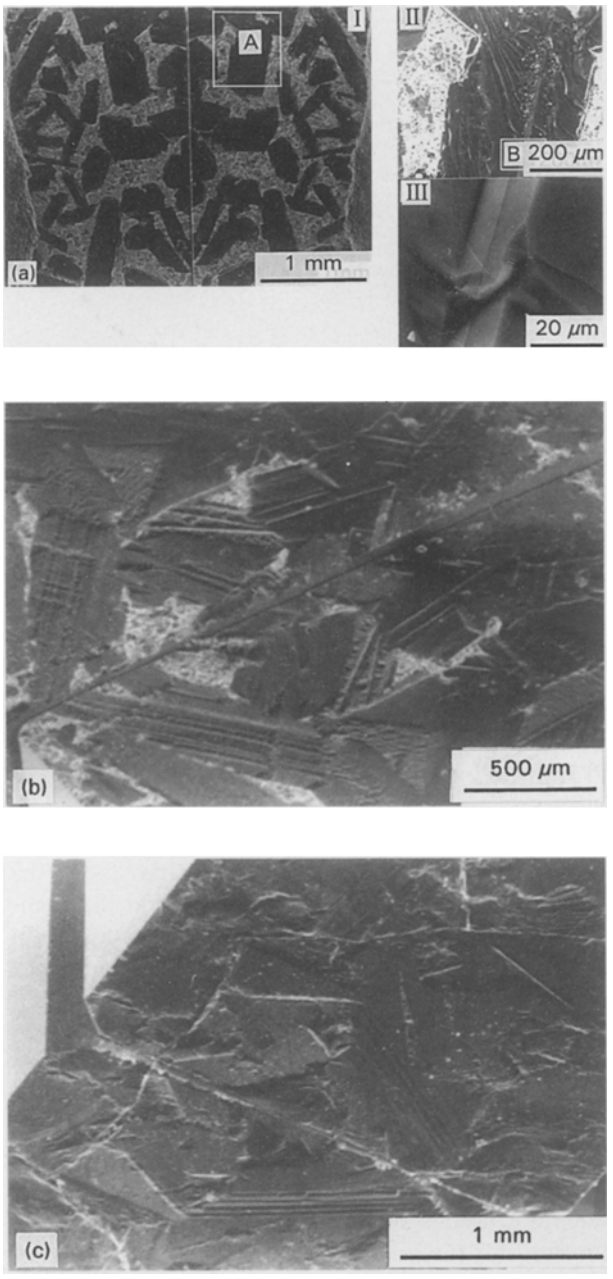

Figure 10 RBSiC–Al joint fracture surfaces showing Si braze slabs cleavage markings: (a) 800 °C, 90 min: (II) detail of zone **A** on (I) and (III) detail of zone **B** on (II); (b) 880 °C, 30 min and (c) 1000 °C, 0 min.

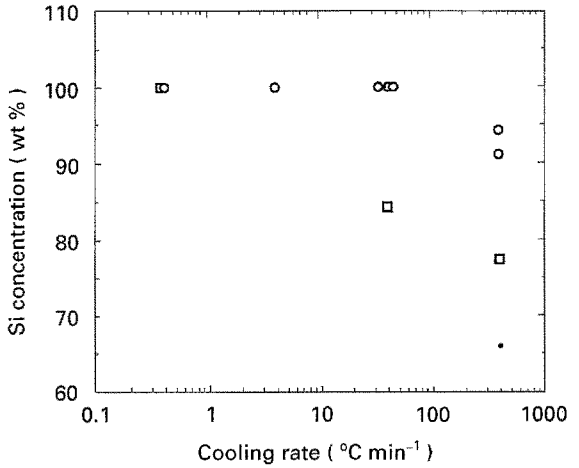

Figure 11 RBSiC vacuum brazed with Al. Variation of the Si concentration in the braze layer with cooling rate: (○) 1000 °C, 30 min; (□) 880 °C, 30 min; (●) 1000 °C, 0 min.

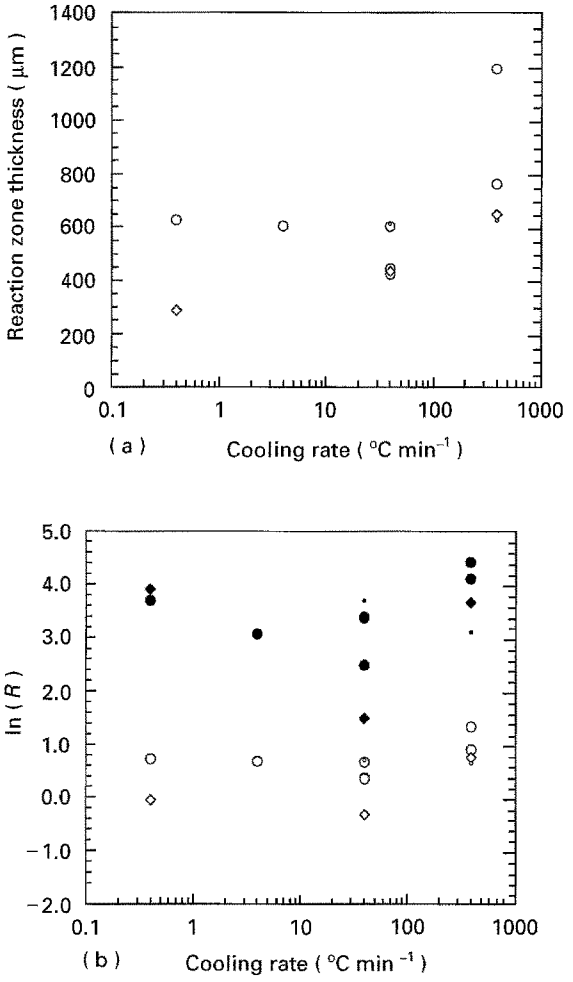

Figure 12 RBSiC vacuum brazed with Al. Variation of (a) reaction zone thickness: (○) 1000 °C, 30 min; (◇) 880 °C, 30 min, (○) 1000 °C, 0 min; and (b) ln(R) with cooling rate: (○) R_i, 1000 °C, 30 min; (●) R_f, 1000 °C, 30 min; (◇) R_i, 880 °C, 30 min; (◆) R_f, 880 °C, 30 min; (○) R_i, 1000 °C, 0 min; (●) R_f, 1000 °C, 0 min.

Fig. 13. The 30 min quenched sample (Fig. 13b), shows pockets of the Al–Si eutectic imprisoned between the RBSiC structure and the primary Si braze plates, while the 0 min quenched sample (Fig. 13c) shows extended Al–Si areas with the normal configuration. The same trend is verified at 880 °C.

Si grain size can be assessed through observation of the joint fracture surfaces. With the slow cooled specimens (0.4 °C min^{-1}) large Si plates, bigger than 1 × 1 mm, form (Fig. 14a, c). This size is reduced as the cooling rate increases. At 4 °C min^{-1} (Fig. 14d) crystals approximately 1 × 1 mm form, while, for the natural furnace cooling rate (Fig. 10a, b), slabs around 500 μm long form. For the quenched sample (Fig. 14b, e and f) smaller Si plates, 100–200 μm long, are clearly visible in the structure, surrounded by Al–Si eutectic.

In the 1000 °C–0 min quenched specimen, porous regions could be identified (Fig. 15). Here the braze structure is characterized by primary Si solidified slabs typically 100–200 μm in size (Fig. 14f), but the interslab volume is not filled with the Al–Si eutectic. Instead, small dendrites, growing perpendicularly to the side faces of the broken Si slabs are observed (Fig. 15). This is thought to be due to a solidification

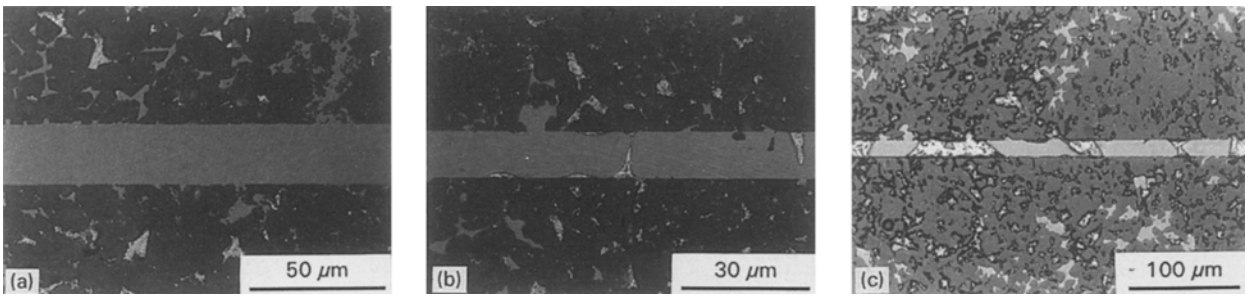

Figure 13 RBSiC–Al joint microstructure vacuum brazed at 1000 °C: (a) 30 min and 0.4 °C min^{-1} cooling rate; (b) 30 min and quenched, and (c) 0 min and quenched. Note the evolution of Al–Si eutectic formation in the braze plane.

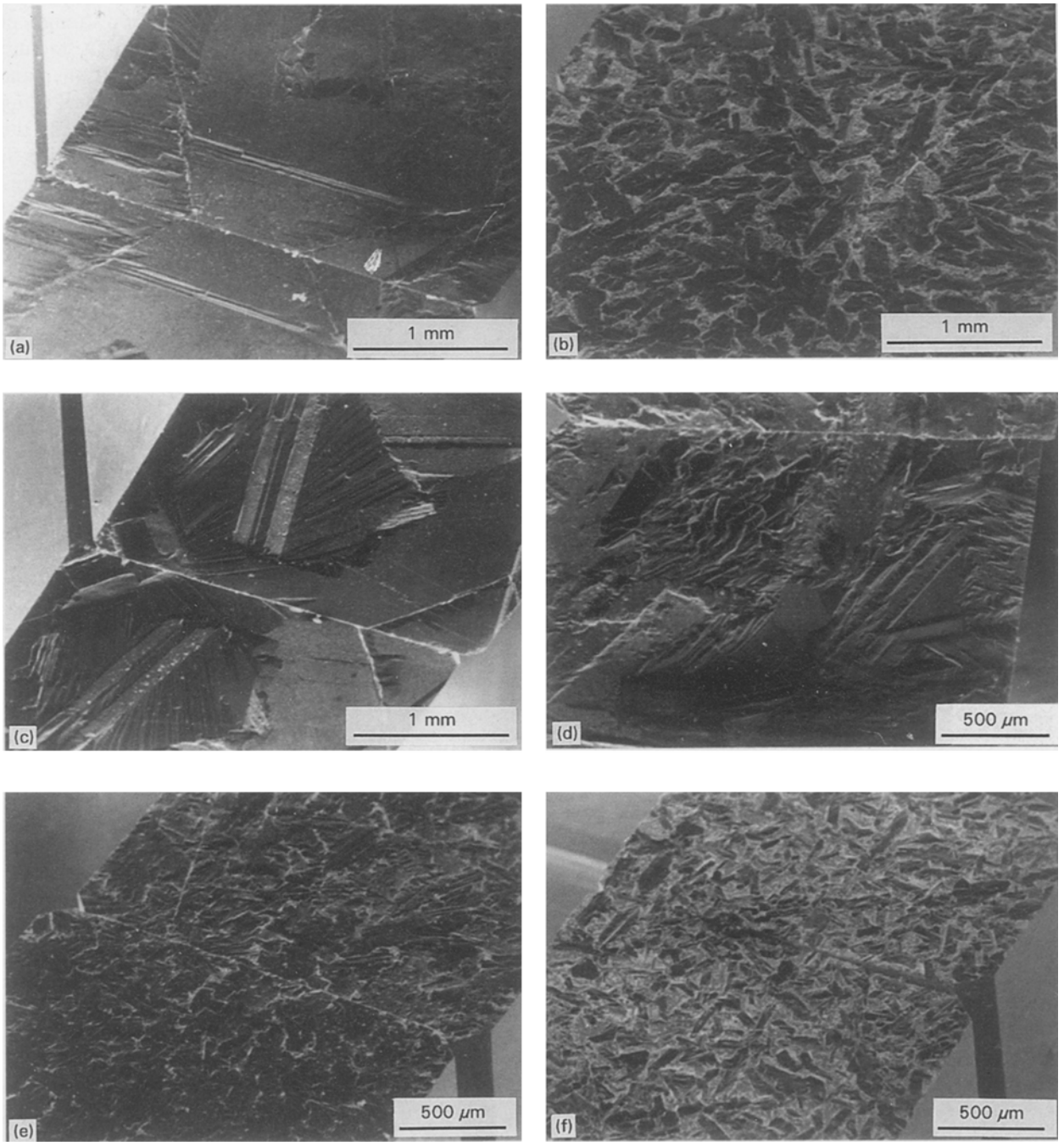

Figure 14 RBSiC–Al joint fracture surfaces showing Si braze grain size: (a) 880 °C, 30 min, 0.4 °C min^{-1} cooling rate; (b) 880 °C, 30 min, quenched; (c) 1000 °C, 30 min, 0.4 °C min^{-1}; (d) 1000 °C, 30 min, 4 °C min^{-1}; (e) 1000 °C, 30 min, quenched; and (f) 1000 °C, 0 min, quenched.

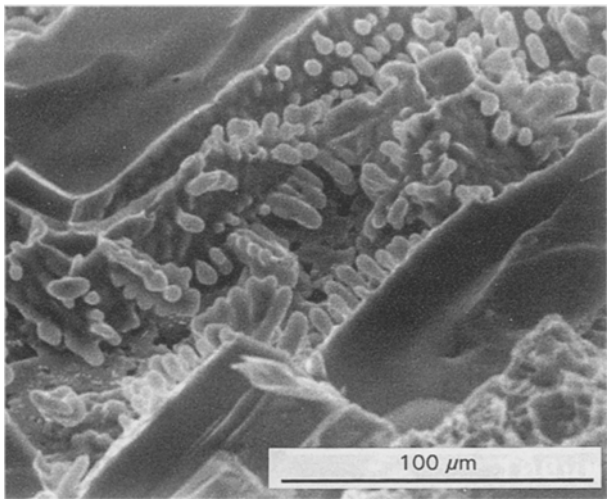

Figure 15 Fracture surface of RBSiC–Al joint vacuum brazed at 1000 °C, 0 min and quenched showing area with porosity and illustrating dendrite growth perpendicular to the Si plate side faces.

feeding problem. Not enough liquid was available in these areas to produce a full dense solid braze film and the void formed after shrinkage.

3.2. Mechanical properties

3.2.1. Room temperature four-point bend tests

The four-point bend test results obtained for the RBSiC–Al brazes are summarized in Table III. They are average values from six to 27 individual tests. Bars were cut from one to four specimens for a given set of brazing conditions.

Crack propagation either occurs along the braze plane or the ceramic–reaction zone boundary, indicating that these areas are weaker than the bulk ceramic and that residual stress has not been relieved by plastic deformation of the metal braze. This is illustrated by the formation of long cracks perpendicular to the joining plane that run from the braze plane into the ceramic–reaction zone boundary (Fig. 16). The residual stresses developed are thought to be generated by the mismatch in thermal expansion coefficient between the Al–Si solid eutectic in the reaction zone and both the SiC and Si. Cracks are more frequent when larger amounts of Al–Si eutectic are present in the reaction zone, i.e. at lower brazing temperatures. However, during four-point bend testing, crack initiation and propagation is not related to these pre-existing perpendicular cracks.

The results obtained are also explained by the low toughness of the Si phase and low adhesion strength of the Si–SiC interface. When type B and D fracture surfaces are observed the crack propagation plane either occurs inside the Si braze film, producing the already discussed cleavage markings, or at the braze–ceramic interface. In this case, although the Si braze film replicates almost perfectly the RBSiC surface (polishing scratches are visible in the Si side of the fracture surface, Fig. 17) SiC grain pull-out is rarely observed.

In spite of the scatter in the data some trends in mechanical strength can be proposed. For specimens naturally cooled inside the furnace, the highest strengths are obtained either for 90 min brazing times when the temperature is $\leqslant 880\,^{\circ}C$, or 30 min for higher temperatures (1000–1100 °C). In these cases modulus of rupture (MOR) values above 200 MPa are obtained with standard deviations below 50 MPa. When either longer or shorter brazing intervals are used a net strength decrease is observed. The effect of

TABLE III Room temperature four-point bend strength, MOR, of RBSiC brazed with Al (fracture type is indicated below)

Brazing temperature (°C)	MOR (MPa)				Cooling rate (°C min^{-1})
	Brazing time (min)				
	0	30	90	240	
700	—	—	260 ± 30 E	—	NCR
800	—	—	250 ± 50 B ⟷ E	—	NCR
880	—	70 ± 70 B	—	—	0.4
	—	80 ± 50 B ⟷ D	230 ± 50 E → B	140 ± 50 B	NCR
	—	210 ± 50 B ⟷ E	—	—	Quenched
1000	—	270 ± 50 B	—	—	0.4
	—	200 ± 120 B → (E)	—	—	4
	130 ± 120 B	230 ± 100 B → E	50 ± 30 B → (E)	—	NCR
	120 ± 30 D ⟷ E	190 ± 40 B	—	—	Quenched
1100	—	250 ± 30 B → (E)	—	—	

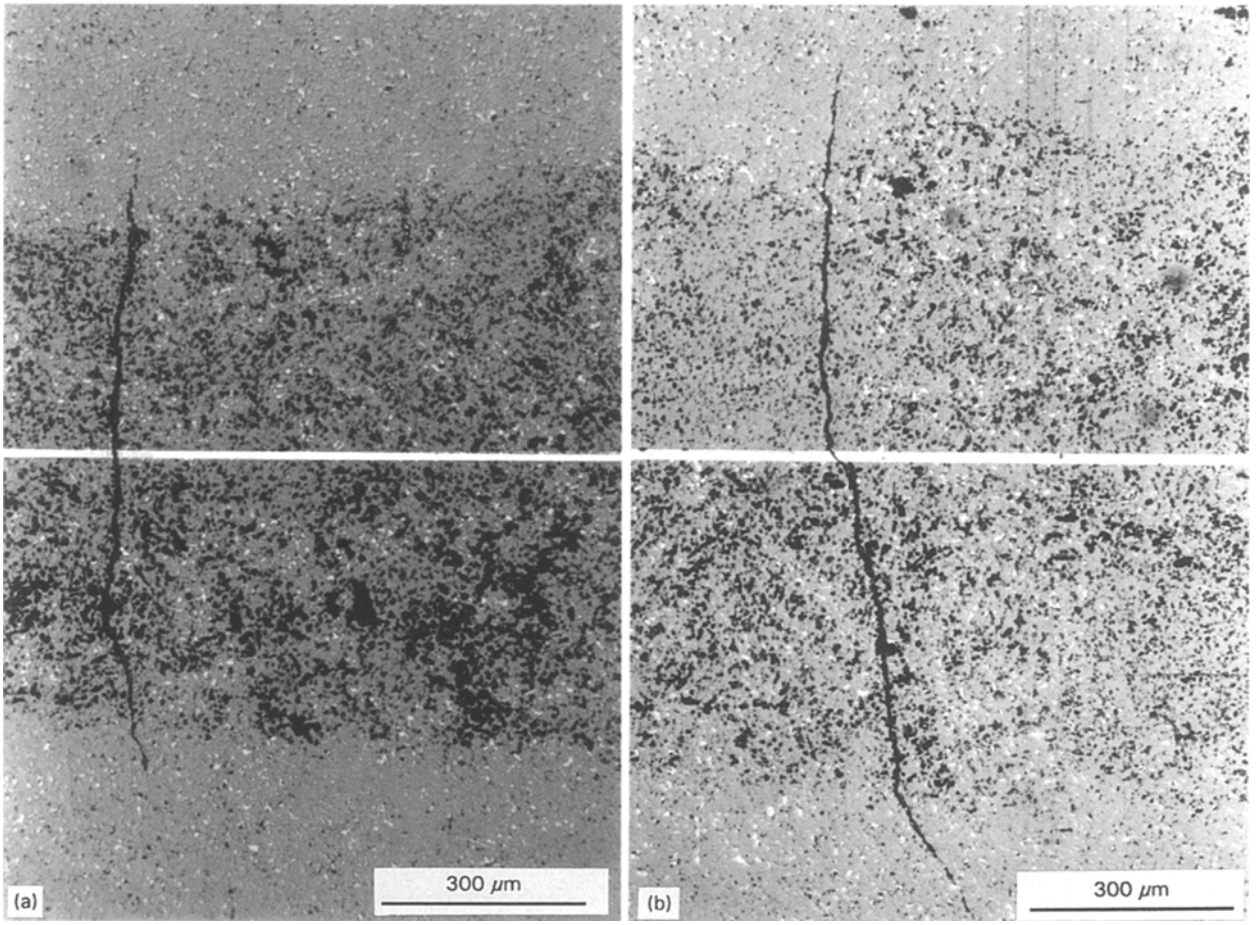

Figure 16 Typical cracks formed in the braze structure due to residual stresses: (a) 700 °C–90 min–NCR, and (b) 1000 °C–30 min–NCR.

cooling rate is difficult to establish and both increases and decreases in strength are observed either for faster or slower cooling rates depending on brazing conditions.

3.2.2. Elevated temperature four-point bend tests

Four-point bend tests were carried out at 300, 500 and 700 °C to assess the high temperature potential of the high silicon content braze films. Two brazing conditions were selected: 800 °C–90 min–NCR, and 1000 °C–30 min–NCR. These produce 75 and 100% Si concentrations in the braze film, respectively. The results obtained are summarized in Table IV. These represent single results or average values from two test bars.

For the 800 °C specimen a decrease in strength is observed when temperatures higher than room temperature are used. At 700 °C it drops significantly with the melting of the Al–Si eutectic present in the braze plane. At this temperature extensive melted areas are observed on the fracture surface (Fig. 18a) and although some cleavage of the Si phase is still visible (Fig. 18b) liquid bridging between the two fracture surfaces is clearly identified (Fig. 18c). For the specimens brazed at 1000 °C no decrease in strength is detected when temperatures higher than room temperature are used. At 700 °C fracture occurs at the ceramic–reaction zone boundary. When the fracture surface is examined at high magnification, melting is observed in some areas and Al–Si droplets are clearly visible wetting SiC grains (Fig. 19a). In other areas fracture goes across the ceramic and no melted areas are detected (Fig. 19b). Although more reliable data are needed, particularly from creep tests, these results tend to show that the temperature capability of the Al brazes, due to this kind of transient liquid phase (TLP) joining that produces pure Si braze films, can be extended at least to 700 °C.

3.3. Summary of main results obtained

The most unexpected result is the formation of a braze layer with Si concentrations well in excess of liquid saturation at the brazing temperature according to the Al–Si binary phase diagram. This deviation increases with increasing temperature and with decreasing cooling rates. 100% Si films can be produced at 880 °C for 0.4 °C min^{-1} cooling rate, or at 1000 °C for cooling rates up to $\approx 20-40$ °C min^{-1}. Brazing time seems to have little influence on this behaviour and, at 1000 °C, a 100% Si braze layer can be produced even for zero holding times.

Due to the formation of an Al–Si liquid replacing the interconnected Si phase of the RBSiC ceramic, an Al rich reaction zone forms in the ceramic on both sides of the braze layer. Its thickness is in excess of the maximum theoretical values, particularly at high temperature. Brazing time and cooling rate have little

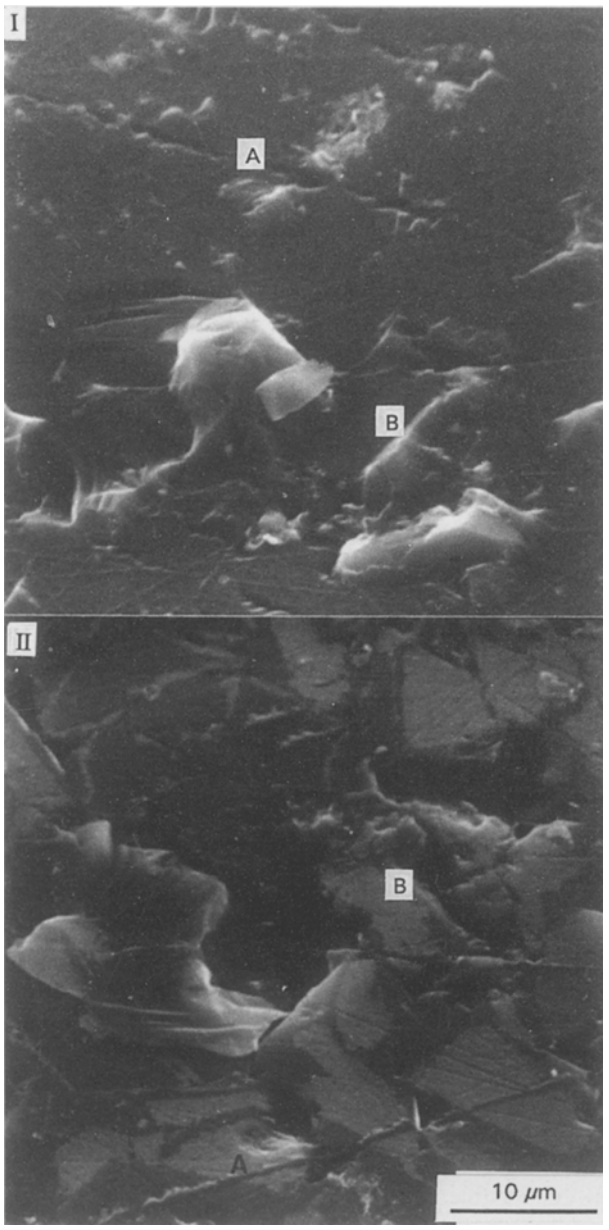

Figure 17 Fracture surface pairs showing adhesion failure and perfect replication of the ceramic surface by the Si braze layer: 1000 °C–30 min–NCR.

TABLE IV Higher temperature four-point bend strength, MOR, of RBSiC brazed with Al (fracture type is indicated below)

Brazing conditions	MOR (MPa)			
	Testing temperature (°C)			
	r.t.	300	500	700
800 °C–90 min–NCR	250 ± 50	160	155	90 ± 20
	B	B	D	(B)
1000 °C–90 min–NCR	230 ± 100	200	180	220 ± 10
	B → E	B	E	E

effect except for the quenched samples, where a net thickness increase is found.

For a given brazing temperature the grain size of the Si phase in the braze layer, as assessed by cleavage marking on fracture surfaces, is controlled by the cooling rate. On cooling from 1000 °C, at 0.4 °C min^{-1}, Si plates greater than 1 × 1 mm with the thickness of the braze film are typically observed, whereas in the quenched samples 100–200 μm long slabs, or even smaller, form.

This brazing method produces joints of useful strength at about 50% of the ceramic's room temperature value. What is more interesting is the result that this strength is retained to 700 °C when the braze is fabricated at 1000 °C. These high, temperature stable, strengths are presumably related to the high Si content of the resulting braze layer and the dispersion of the Al as eutectic islands in the reaction zone.

4. Discussion

Four possible mechanisms by which the formation of a pure Si layer during brazing can be explained will be discussed.

4.1. Preferential solidification of the braze layer due to thermal gradients

Given the geometry of the furnace, the thermal profile generated on cooling is expected to produce isotherms perpendicular to the main alumina tube axis, with the cooler areas corresponding to its outer regions. This will produce symmetric thermal profiles in the joining assembly. Hence, the braze layer is expected to be the last zone to solidify. To assess further the influence of external thermal profiles an experiment was carried out at 1000 °C for 30 min where both the jig–furnace and jig–braze assemble positions were displaced to produce a modified cooling pattern, i.e. a thermal gradient of constant sign across the braze. No difference could be identified between this specimen and those performed with the normal configuration.

It may also be thought that some effect could arise from faster heat conduction through the braze film, compared to conduction through the RBSiC bulk ceramic, given the presence of the Al–Si liquid and solid Si. However, that layer is too thin to disturb considerably the thermal profile. In addition, at high temperature, the differences in thermal conductivity between Al, Si and SiC are relatively small, particularly if an Si rich Al–Si liquid is considered [36–40].

Hence, this hypothesis is rejected. The thermal gradient profiles are considered to have no effect on the observed high Si concentration of the braze layer.

4.2. Increased equilibrium Si concentration because of the formation of an Al–C–Si ternary liquid

Carbon has a much higher solubility in Al–Si liquids than in pure Al [18]. Although this could not be quantified, at 1000 °C carbon concentrations as high as 1 at % are possible for Al–Si liquids with Si concentrations greater than the eutectic. So, in the presence of high Si content Al–Si liquids SiC will dissolve until carbon saturation occurs. This may change the maximum equilibrium Si concentration of the Al–Si–C liquid for a given temperature.

The eutectic temperature in the C–Si binary phase diagram is only 10 °C below the Si melting point and

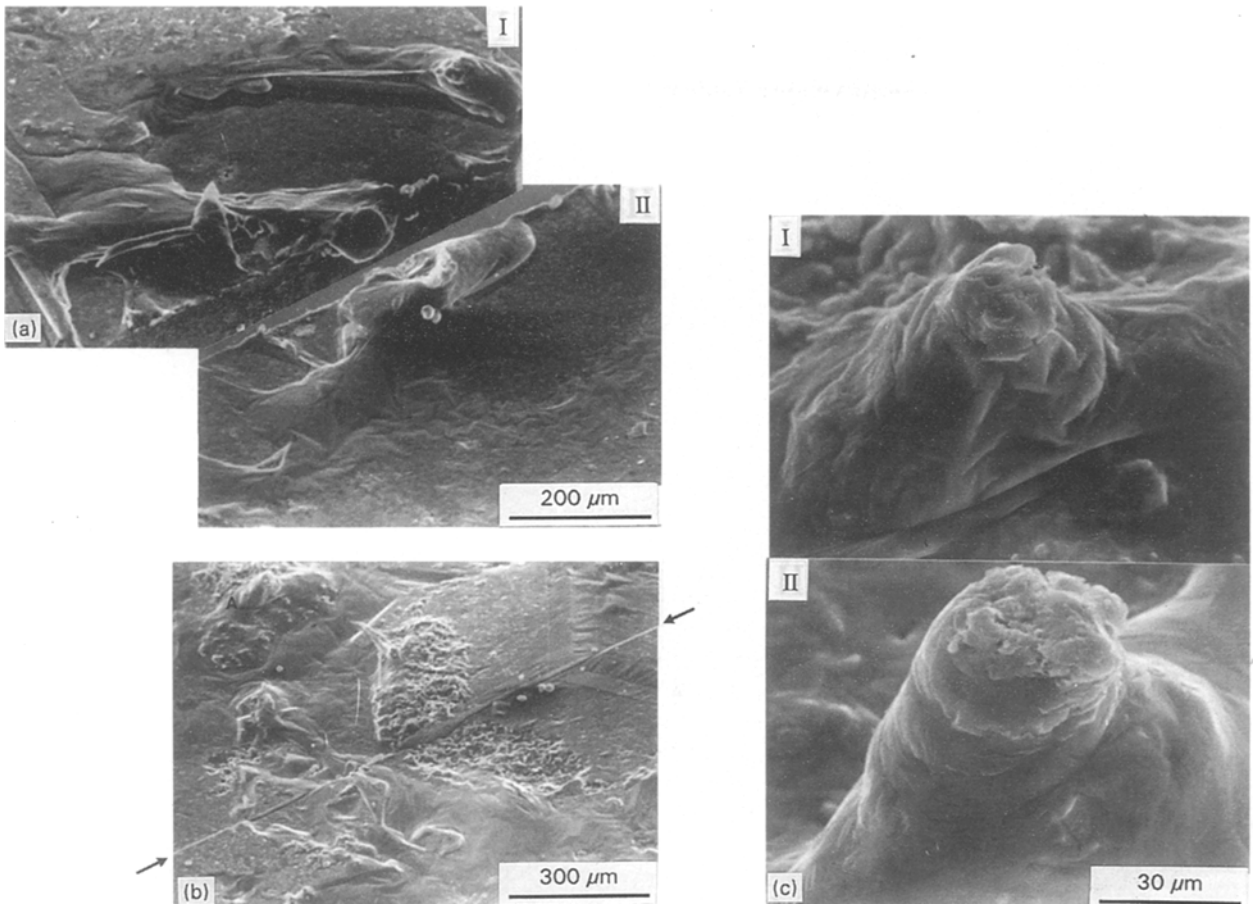

Figure 18 A 700 °C fracture surface of RBSiC–Al vacuum brazed at 800 °C–90 min–NCR: (a) pair showing extensive liquid formation at the braze film; (b) pair, general view presenting Si cleavage and melted areas; and (c) bridge marked A in (b).

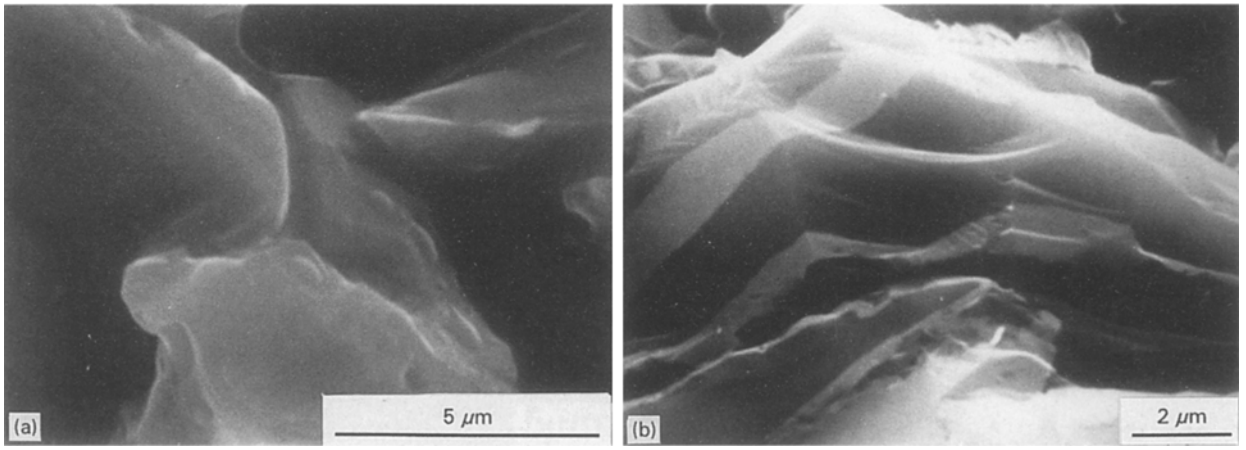

Figure 19 A 700 °C fracture surface of RBSiC–Al vacuum braze at 1000 °C–30 min–NCR showing: (a) droplet formation due to melting of the Al–Si eutectic at the ceramic reaction zone, and (b) fracture across the ceramic.

its composition has 0.75–0.5 at % dissolved carbon [41]. Also the temperature of the ternary Al–C–Si eutectic is only 1–2 °C below the Al–Si binary eutectic [12]. No further information on the depression of the liquidus temperature of Al–Si alloys by the addition of carbon has been reported. It is not then obvious that the addition of carbon will noticeably depress the liquidus temperature of high Si content Al–Si melts and increase the equilibrium Si concentration. Moreover, when the wetting of RBSiC by pure Al was studied [42], the Si concentration of the droplets formed at different temperatures was found to be lower than the saturation value of the Al–Si binary melts, further questioning the validity of this hypothesis.

Three more experiments were designed to investigate the hypothesis.

1. A normal RBSiC–Al braze assembly was prepared, but a 150 μm wide, 1 mm deep notch was cut in the upper RBSiC stub perpendicular to the braze plane and across a diameter of its surface. A 1000 °C, 30 min and the natural cooling rate of the furnace were selected for the brazing conditions and, given these conditions, the Al–Si liquid was expected to infiltrate the notch and crystallize to produce a pure Si

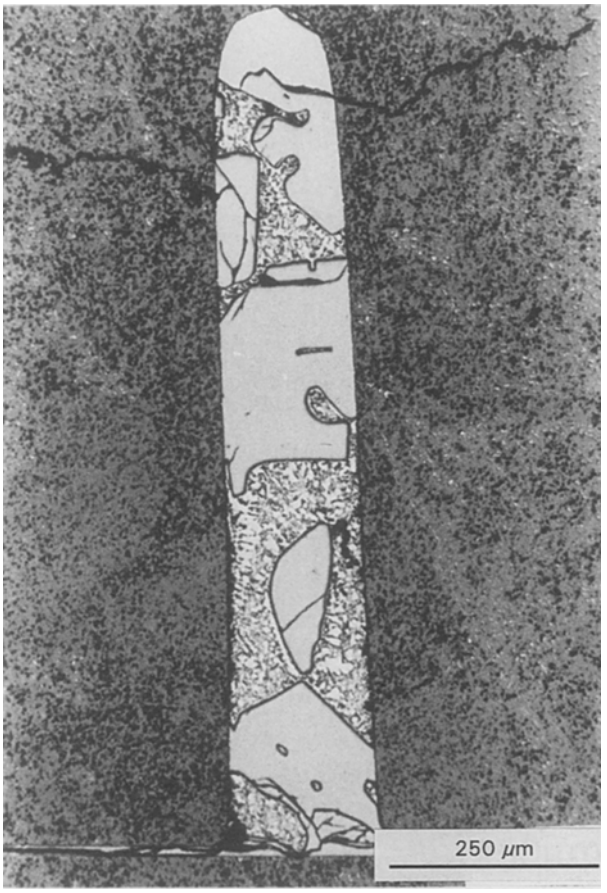

Figure 20 RBSiC–Al vacuum brazed at 1000 °C for 30 min and naturally cooled inside the furnace showing an Si braze film (bottom of micrograph) and a crystallized hypereutectic Al–Si alloy in the notch.

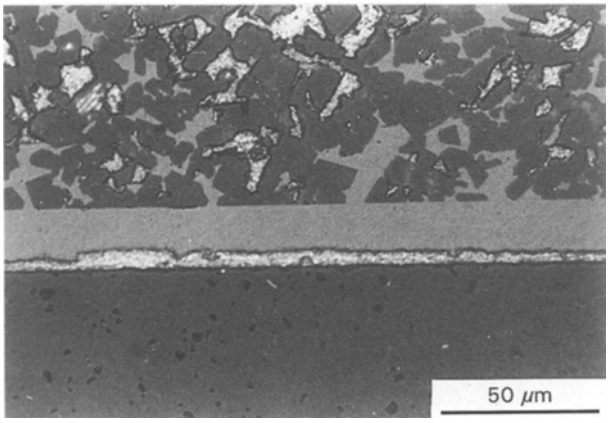

Figure 21 RBSiC–Al–α–SSiC vacuum brazed at 1000 °C for 30 min and naturally cooled inside the furnace showing the formation of an Al–Si layer on the α-SSiC side of the braze film.

film. However, the Si concentration measured, although in excess of the binary Al–Si saturation, was only 62.5%. At the braze layer a pure Si film still forms (Fig. 20).

2. An α-SSiC stub was used to replace one of the RBSiC brazing specimens to form an α-SSiC–Al–RBSiC assembly. An increase in the ceramic reaction zone thickness was observed as expected, from the normal 400–600 to 1000 μm (in this case only one side of the braze assembly is available to supply free Si to saturate the melt). Extended pockets of Al–Si, or even

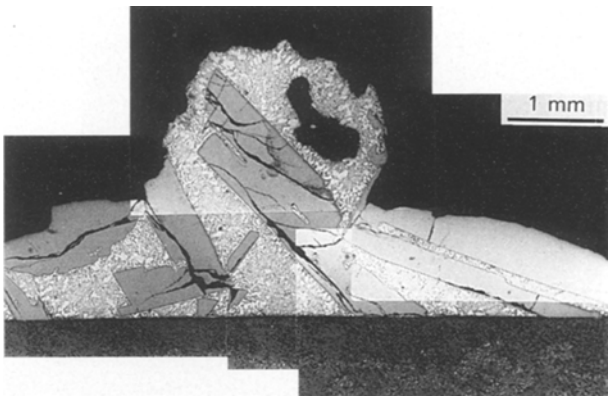

Figure 22 Al–Si droplet formed between pure Al and RBSiC after 24 h at 1000 °C.

a complete eutectic layer, form in the braze film in contact with the α-SSiC. However, a Si layer is still seen on the RBSiC side (Fig. 21).

3. Finally a 95 mg Al stub was left in contact with RBSiC for 24 h at 1000 °C. In this case, from the size of the ceramic reaction zone a Si concentration around 55% was estimated. The solidified droplet shows a considerable amount of Al–Si eutectic (Fig. 22).

These results confirm that the change in the equilibrium Si concentration due to the formation of a carbon saturated Al–C–Si ternary liquid cannot *per se* explain the formation of pure Si braze films at high temperature. Although some increase in the liquid Si content is expected, no evidence was obtained to sustain this hypothesis.

4.3. Preferential growth of Si plates in the braze layer

The solidification of hypereutectic Al–Si alloys is known to produce very coarse primary Si crystals [43, 44]. In a physically unconstrained volume of liquid, coarse Si plates crystallize upon cooling and their thickness increases with the silicon concentration of the melt. At 1000 °C, for an Si saturated Al–Si alloy (≈45% Si) plates thicker than 200 μm are expected to form when the natural cooling rate is used (20–40 °C min^{-1}). The formation of these coarse plates is attributed [43, 44] to a reduced Si nucleation rate, to the anisotropy of Si surface energy, and to a twin plane reentrant edge (TPRE) growth mechanism, e.g. [45, 46].

During RBSiC–Al brazing, if sufficient time is allowed at the joining temperature, a homogeneous Al–Si hypereutectic liquid, with an Si concentration similar to the equilibrium value given by the Al–Si binary phase diagram, will be formed. This liquid replaces the Si phase of the RBSiC material, and forms a continuous network extending through the SiC skeleton (the ceramic reaction zone) and the braze layer.

Upon cooling, Si nuclei growth inside the ceramic reaction zone is constrained in all directions by impingement with the SiC skeleton. Accordingly, the TPRE growth mechanism nuclei are expected to have fast growth in the ⟨1 1 2⟩ directions (directions in the

{1 1 1} low surface energy planes), e.g. [45, 46], but this is limited to the typical size of the ceramic reaction zone channels, $< 10\ \mu m$. Although low energy large angle branching mechanisms have been described [45, 46] that will allow further growth of the Si plates, this will again be constrained by impingement. Further growth is expected to occur by slow thickening of the Si plates normal to the {1 1 1} planes.

Contrarily, the nuclei formed in the braze layer are only constrained in one-dimension. Those crystals with {1 1 1} planes orientated parallel, or nearly parallel, with the braze plane, or those that, by the TPRE small or high angle branching mechanism, produce Si plates branches close to that orientation, are free to grow unrestrained in the braze plane. Given the relatively small thickness of the braze film, 15–60 μm, when compared to the typical width of the primary Si plates formed for normal cooling rates, it is not surprising that single Si plates grow along the braze layer covering its entire thickness.

Both the preferential growth of Si primary plates in the braze layer, which is favoured by fast Si liquid diffusion from the adjacent reaction zone areas, and the constrained growth of Si in the ceramic reaction zone, play a dominant role in the increased Si concentration in the braze film. A low nucleation rate, preferential fast growth of Si in the braze plane and fast Si liquid diffusion are the key phenomena that support the formation of high Si or even pure Si joining interlayers during Al–RBSiC brazing.

The experimental evidence supports this hypothesis. Big Si plates were identified in the braze layer, with the {1 1 1} cleavage planes parallel to the braze plane (Figs 10 and 14) indicating that two-dimensional crystal growth has taken place. Evidence of small angle branching, also responsible for fast growth, producing {1 1 1} cleavage planes with a small angle to the ceramic surface, has been repeatedly observed (Fig. 23). When the nucleation rate is increased by gas quenching, smaller primary Si plates form (Fig. 14b, e and f) and reduced amounts of Si are present in the braze layer.

When the supply of silicon to the braze layer, by liquid diffusion from the ceramic reaction zone, is hindered, increased amounts of Al–Si eutectic or porosity develop in that layer. This is the case for the α-SSiC–Al–RBSiC joint, where abundant Al–Si eutectic forms along the SSiC side of the braze layer (Fig. 21). The supply of Si is physically hindered by the formation of Al–Si liquid pockets between the Si plates that develop in the braze film and the α-SSiC surface. These have limited connections to the Si rich Al–Si reaction zone liquid. The same also applies for the quenched samples. Here, besides the nucleation

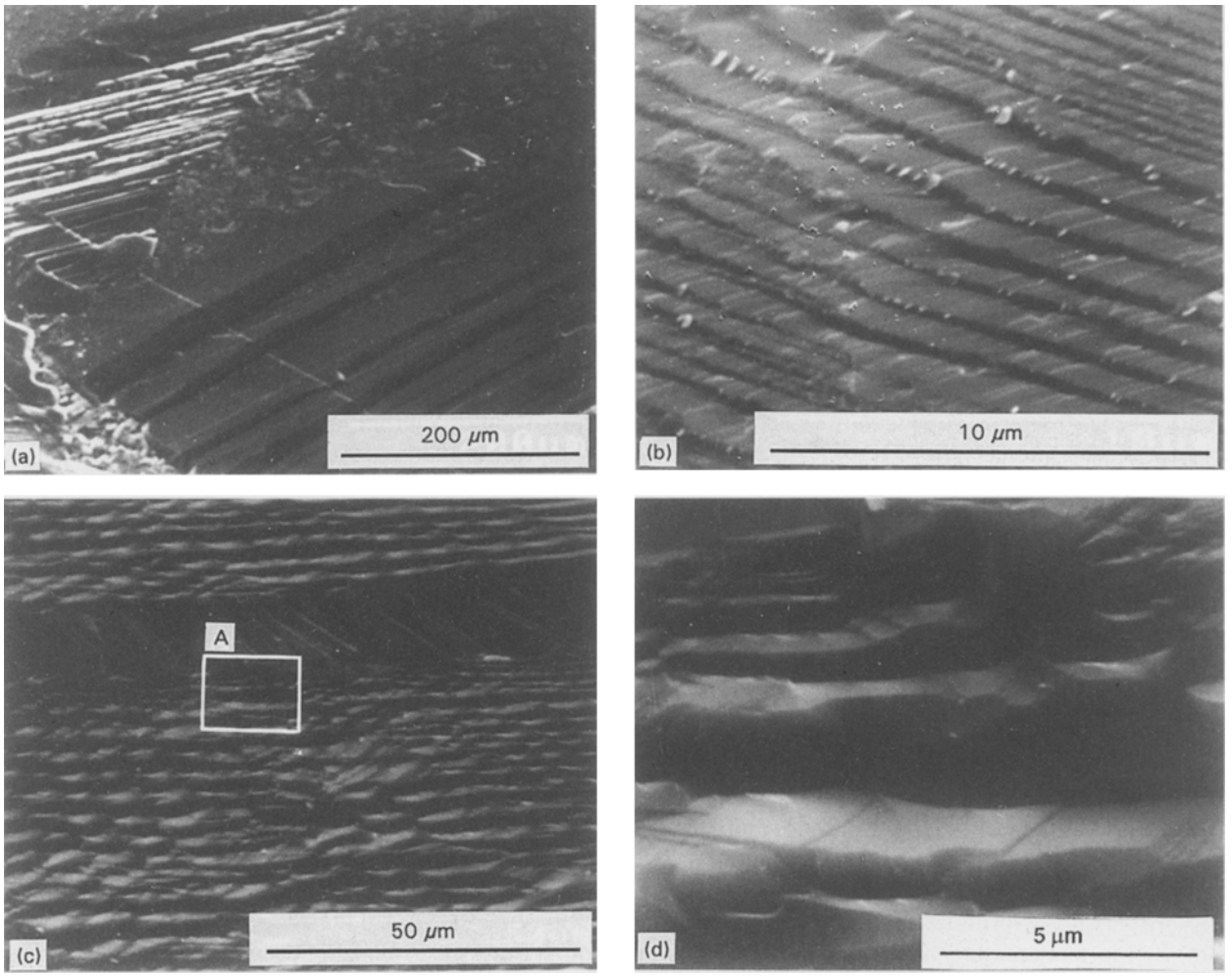

Figure 23 RBSiC joint fracture surface showing {1 1 1} cleavage facets making a small angle with the ceramic surface: (a) 1000 °C–30 min–0.4 °C min^{-1}; (b) 1000 °C–30 min–NCR–4.5 μm Al evaporated braze film; (c) 1000 °C–90 min–NCR; and (d) detail of the zone **A** on (c).

factor, fast growth of the Si plates due to increased undercooling and Si liquid diffusion limits the amount of Si that can be supplied to the solid–liquid interface. In the presence of a non-homogeneous liquid with a lower Si total concentration, as is thought to be the case for the 1000 °C quenched, zero soaking time experiment, this effect is further magnified (Figs 11, 14d and f).

4.4. Capillary and surface-phenomena mechanisms

In the Al–Si–SiC system, low contact angles ($\approx 25°$) are obtained at 1100 °C for alloys with compositions near the eutectic. Although low angles are still observed for higher Si concentrations, up to 45%, a gradual increase in the contact angle is observed [18]. Given the high specific area of the SiC skeleton phase, during brazing, this effect may contribute to the preferential formation of Al–Si eutectic areas in the ceramic reaction zone and so increase the Si concentration in the braze layer. However, the importance of this phenomenon in the establishment of very high Si braze films is difficult to assess.

It was determined experimentally that the ceramic reaction zone is established very quickly (brazing time has no effect on it). The establishment of these zones is controlled both by Si dissolution and liquid infiltration by capillarity. If one considers the equation for capillary rise, an approximate relation can be established between the size of the reaction zone channels, considered as small capillaries with circular cross-sections, and the expected capillary rise, h. Considering the typical values of γ_{Al} and θ and the Al–Si liquid density one has

$$h \approx \frac{70}{r}\,(\mu m) \qquad (2)$$

Capillary rise assumes considerably different values when either coarse, $r \geqslant 10\ \mu m$, or small channels, $r \leqslant 0.5\ \mu m$, are considered and that the order of magnitude of these values is similar to the thickness of the ceramic reaction zones formed in the RBSiC material. This effect may be enhanced by the rapid kinetics of Si solution and establishment of the reaction zone, which may lead to preferential growth through smaller channels. This may leave behind some undissolved coarser Si areas. The assumption so far made, that all free Si existing in the ceramic reaction zone is dissolved, may not be true which could explain the excess reaction zone thickness so often observed. The formation of low and high Si Al–Si eutectic regions in the reaction zone and the preferential occupation of the thinner connect matrix areas by the eutectic (Fig. 9) may also be partially explained by this capillary and surface energy effect.

Thus one concludes that the dominant mechanism responsible for the formation of the braze microstructure is the preferential unrestrained solidification growth of Si plates on the braze plane, supported by fast liquid Si diffusion. An eventual Si solubility increase in the liquid because of the formation of a ternary Al–C–Si melt, the preferential penetration of the liquid through the thinner channels of the interconnected Si–RBSiC phase, by capillary action, and the preferential establishment of SiC–Al–Si interfaces (instead of SiC–Si) may also contribute to the formation of the braze microstructures.

5. Conclusions

1. When Al is used to join RBSiC to itself, a thin Si rich braze film and a thick ceramic reaction zone are observed. The Si concentrations of these films are well in excess of the Si liquid saturation at the brazing temperature, predicted by the Al–Si phase diagram. 100% Si films can be produced below 900 °C. The thickness of the reaction zone was found to be in excess, according to an Al mass balance and assuming that all Si in the zone is dissolved into the Al–Si liquid.

2. The silicon concentration in the braze film depends on brazing temperature and cooling rate. Brazing time has little influence. 100% Si films were obtained at 880 °C for 0.4 °C min^{-1} cooling rate and, at 1000 °C, pure Si films are obtained even for samples naturally cooled inside the furnace (≈ 20–40 °C min^{-1}).

3. The thickness of the reaction zone is established very quickly (1–2 min) and is thought to increase with temperature from ≈ 200–$400\ \mu m$ at 880 °C to ≈ 400–$600\ \mu m$ at 1000 °C and to $\approx 1200\ \mu m$ at 1100 °C. Brazing time and cooling rate seem to have little influence on reaction zone thickness.

4. This kind of transient liquid phase joining, where a higher melting point alloy is obtained at the braze film after joining (in the extreme case pure Si replaces pure Al), may be explained by the combined effect of three mechanisms: the dominant mechanism is thought to be the preferential unrestrained solidification growth of Si plates on the braze plane. This is supported by fast liquid Si diffusion and for the eventual Si solubility increase in the liquid due to the formation of a ternary Al–C–Si melt. Capillarity, and the preferential penetration of the liquid through the thinner channels of the interconnected Si–RBSiC phase, and a surface energy effect due to the preferential establishment of SiC–Al–Si interfaces (instead of SiC–Si interfaces) may also contribute to the formation of the braze microstructures.

5. The room temperature four-point bend strength of the joints formed present a larger scatter than that determined for the SSiC–Al joints. However, for specimens naturally cooled inside the furnace, brazing times of 90 min for brazing temperatures below 900 °C and 30 min for temperatures $\geqslant 1000$ °C produce reasonably reliable results. In these cases MOR values above 200 MPa with standard deviations below 50 MPa are obtained. Due to the formation of pure Si braze films the temperature capability of Al brazes is extended. Specimens joined at 1000 °C for 30 min and naturally cooled inside the furnace show a four-point bend strength of over 200 MPa at 700 °C.

6. References

1. M. G. NICHOLAS, in: "Joining Ceramics Glass and Metal", edited by W. Kraft (DGM Verlag, Oberursel, 1989) pp. 185–190.
2. M. G. NICHOLAS and D. A. MORTIMER, *Mater. Sci. Technol.* **1** (1985) 657.
3. C. R. GOSTELOW and J. E. RESTALL, *Proc. Brit. Ceram. Soc.* **22** (1973) 117.
4. T. ISEKI, K. ARAKAWA and H. SUZUKI, *J. Mater. Sci. Lett.* **15** (1980) 1049.
5. R. R. KAPOOR and T. W. EAGAR, *Ceram. Eng. Sci. Proc.* **10** (1989) 1602.
6. *Idem, J. Amer. Ceram. Soc.* **72** (1989) 448.
7. J. K. BOADI, T. YANO and T. ISEKI, *J. Mater. Sci.* **22** (1987) 2431.
8. T. YANO, H. SUEMATSU and T. ISEKI, *ibid.* **23** (1988) 3362.
9. P. BATFALSKY, J. GODZIEMBA-MALISZEWSKI and R. LISON, in "Joining Ceramics, Glass and Metal", edited by W. Kraft (DGM Verlag, Oberursel, 1989) pp. 81–88.
10. K. SUGANUMA, T. OKAMOTO, M. KOIZUMI and M. SHIMADA, *J. Amer. Ceram. Soc.* **67** (1984) c256.
11. J.-C. VIALA, P. FORTIER, C. BERNARD and J. BOUIX, in Proceedings of the First European Conference on Composite Materials, Bordeaux (1985) pp. 583–588.
12. J.-C. VIALA, P. FORTIER and J. BOUIX, *J. Mater. Sci.* **25** (1990) 1842.
13. A. S. ISAIKIN, V. M. CHUBAROV, B. F. TREFILOV, V. A. SILAEV and Y. A. GORELOV, *Metal Sci. Heat Treatment* **22** (1980) 815.
14. T. ISEKI, T. MARUYAMA and T. KAMEDA, *Proc. Brit. Ceram. Soc.* **34** (1984) 241.
15. D. J. LLOYD, H. LAGACE, A. McLEOD and P. L. MORRIS, *Mater. Sci. Eng.* **107A** (1989) 73.
16. H. NAKAE, K. YAMAMOTO and K. SATO, *Mater. Trans. JIM* **32** (1991) 531.
17. V. LAURENT, D. CHATAIN and N. EUSTATHOPOULOS, *J. Mater. Sci.* **22** (1987) 244.
18. A. C. FERRO and B. DERBY, *Acta Metall. et Mater.* **43** (1995) 3061.
19. A. KHONO, T. YAMADA and K. YOKOI, *J. Jpn. Inst. Metals* **49** (1985) 876.
20. T. ISEKI, K. YAMASHITA and H. SUZUKI, *Yogyo-Kyokai-Shi* **91** (1983) 11.
21. T. ISEKI, T. KAMEDA and T. MARUYAMA, *J. Mater. Sci.* **19** (1984) 1692.
22. K. SUGANUMA, Y. MIYAMOTO and M. KOIZUMI, *Ann. Rev. Mater. Sci.* **18** (1988) 47.
23. O. M. AKSELSEN, *J. Mater. Sci.* **27** (1992) 1989.
24. A. SUZUMURA, T. ONZAWA, Y. ARATA, A. OOMORI and S. SANO, *Kovonngakkai-Shi* **13** (1987) 43.
25. J. D. WHITTENBERGER, T. J. MOORE and D. L. KURUZAR, *J. Mater. Sci. Lett.* **6** (1987) 1016.
26. H. GRÜNAUER, K. SCHWEIßANLAGEN and U. ROBOTER, in: "Joining Ceramics, Glass and Metal", edited by W. Kraft (DGM Verlag, Oberursel, 1989) pp. 185–190.
27. B. DERBY and E. R. WALLACH, *Metal. Sci.* **16** (1982) 49.
28. W. KRAFT (editor), "Joining Ceramics, Glass and Metal" (DGM Verlag, Oberursel, 1989).
29. M. G. NICHOLAS (editor), "Joining of Ceramics" (Chapman & Hall, London, 1990).
30. T. ISEKI, K. YAMASHITA and H. SUZUKI, *J. Amer. Ceram. Soc.* **64** (1981) c13.
31. M. NAKA, T. SAITO and I. OKAMOTO, *J. Mater. Sci.* **26** (1991) 1983.
32. *Idem, J. Mater. Sci. Lett.* **6** (1987) 875.
33. J. L. MURRAY and A. J. McALISTER, *Bull. Alloy Phase Diag.* **5** (1984) 74.
34. D. J. CLINTON, L. A. LAY and R. MORRAL, *NPL Report Chem.* **113** (1980) 1.
35. U. SCHWABE, L. R. WOLFF, F. J. LOO and G. J. ZIEGLER, *Eur. Ceram. Soc.* **9** (1992) 407.
36. E. A. BRANDES (editor), "Smithells Metal Reference Book", 6th Edn (Butterworth, London, 1983).
37. D. R. LIDE (editor), "CRC Handbook of Chemistry and Physics", 71st Edn (CRC Press, Boston, MA, 1990) pp. 5.70–1.
38. "Inspec, Properties of Silicon", Emis Data Reviews Series No. 4, edited by T. H. Ning and C. Hilsum (The Institute of Electric Engineers, 1988).
39. M. L. TORTI, R. A. ALLIEGRO, D. W. RICHERSON, M. E. WASHBURN and G. Q. WEAVER, *Proc. Brit. Ceram. Soc.* **22** (1973) 129.
40. W. GEORGE, *ibid.* **22** (1973) 147.
41. R. W. OLESINSKI and G. J. ABBASCHIAN, in: "Binary Alloy Phase Diagrams", Vol. 1, 2nd Edn, edited by T. B. Massalski (ASM International, Metals Park, OH, 1990) pp. 882–883.
42. A. C. FERRO, PhD thesis, Oxford University (1992).
43. W. KURZ and D. J. FISHER, "Fundamentals of Solidification" (Trans. Tech. Ltd, Aedermannsdorf, 1989) pp. 122–295.
44. C. WEISS-JAND LOPER, *Trans. AFS.* Paper 32 (1987).
45. M. SCHAMSUZZOHA and L. M. HOGAN, *J. Cryst. Growth* **76** (1986) 429.
46. M. SCHAMSUZZOHA, L. M. HOGAN, D. J. SMITH and P. A. DEYMIER, *ibid.* **112** (1991) 635.

Received 25 April
and accepted 24 May 1995